beads would phase-separate into double-walled microspheres. Bead size appeared to have little effect on whether or not phase-separation would occur. When examined at higher magnification in the light microscope, it became apparent that in each layer, there existed small domains where phase separation had not been complete. For closer examination of these non-phase-separated domains, thin sections (70–80 nm) of the same sample were also cut, stained and examined by TEM. A potassium permanganate stain provided excellent image contrast, allowing us to visualize the different zones of the microspheres. Figure 3*b* shows a TEM micrograph of thin sections of polystyrene/poly(lactic acid) microspheres. The outer wall of the microspheres was pale, and contained semi-crystalline or spherulitic domains. The inner-core phase stained intensely and showed a fibrillar matrix. Circular inclusions in the outer wall apparently contained material resembling the fibrillar matrix of the inner core. Similarly, inclusions in the inner core contained material that failed to separate into the outer layer.

The microspheres were also cross-sectioned with a razor blade in order to study the composition of each layer by FT-IR microscopy. By studying the polymer phases as they appeared in the microspheres, the compositions could be compared to the compositions of the layers formed when the solution was left overnight to completely phase-separate. This comparison showed the extent of phase separation that is obtained during the solvent evaporation process and suggested whether the process should be slowed down by reducing the temperature of the non-solvent bath or the volatility of the solvent in order to allow for more complete phase separation.

Finally, the thermal properties of the double-walled microspheres were studied using DSC. For a completely phase-separated system, the DSC thermogram showed the glass transition temperature and/or melting points of the original polymers. For a system where the polymers were miscible in each other, these temperatures would be shifted, and even merged if the polymers were completely miscible. DSC thermograms of double-walled microspheres showed the two melting points of the original polymers unchanged and distinct, implying that the polymers were immiscible.

Double-layered microspheres can be used to improve present drug delivery technology in a number of ways, including reducing the 'burst effect', fabricating biodegradable and non-degradable spherical devices with zero-order release kinetics and for pulsatile delivery. This new technology for microsphere preparation may have applications in the field of drug or protein delivery. □

Received 25 August; accepted 23 November 1993.

1. Vrancken, M. N. US Patent No. 3523906.
2. Morishita, M. US Patent No. 3960757.
3. Mathiowitz, E., Kline, D. & Langer, R. *J. Scanning Microsc.* **4,** 329–340 (1990).
4. Mathiowitz, E., Saltzman, W. M., Domb, A., Dor, Ph. & Langer, R. *J. appl. Polym. Sci.* **35,** 755–774 (1988).
5. Mathiowitz, E., Dor, Ph., Amato, C. & Langer, R. *Polymer* **31,** 547–555 (1990).
6. Mathiowitz, E. *et al. J. appl. Polym. Sci.* **45,** 125–134 (1992).
7. Madan, P. L. *Drug Dev. Ind. Pharm.* **4,** 95–95–116 (1978).
8. Madan, P. L., Luzzi, L. A. & Price, J. C. *J. phar. Sci.* **61,** 1586–1588 (1972).
9. Heistand, E. N., Wagner, J. G. & Knoechel, E. L. US Patent No. 24899 (1960).
10. Green, B. K. & Schleicher, L. to The National Cash Register Company. US Patent No. 2800457; US Patent No. 2800458 (1963).
11. Mathiowitz, E. & Langer, R. US Patent No. 4861627 (1989).
12. Harkin, W. D. *The Physical Chemistry of Surface Films* (Reinhold, New York, 1952).
13. Torza, S. & Mason, G. *J. Colloid Interface Sci.* **33,** 67–83 (1970).
14. Heller, J., Fritzinger, B. K., Ng, S. Y. & Penhale, D. W. *J. Controlled Release* **1,** 87–95 (1985).
15. Parrott, E. L. *Pharmaceutical Technology* 86–88 (Burgess, Minneapolis, Minnesota, 1970).
16. Parrott, E. L. *Pharmaceutical Technology* 90–91 (Burgess, Minneapolis, Minnesota, 1970).

ACKNOWLEDGEMENTS. We thank NOVA Pharmaceutical for providing the polyanhydrides and J. Heller for donating the poly(ortho ester). This work was supported by the Whitaker Foundation.

Effect of deep-sea sedimentary calcite preservation on atmospheric CO_2 concentration

D. Archer* & E. Maier-Reimer†

*‡ Lamont-Doherty Earth Observatory of Columbia University, Palisades, New York 10964, USA
† Max-Plank-Institut für Meteorologie, Bundesstrasse 7, D-2000 Hamburg 54, Germany

DURING the last glaciation, the atmospheric carbon dioxide concentration was about 30% less than the Holocene pre-industrial value[1]. Although this change is thought to originate in oceanic processes[2], the mechanism is still unclear. On timescales of thousands of years, the pH of the ocean (and hence the atmospheric CO_2 concentration) is determined by a steady-state balance between the supply rate of calcium carbonate to the ocean from terrestrial weathering, and the alteration and removal of carbonate by burial in sediments[2–4]. Degradation of organic carbon in sediments promotes the dissolution of calcium carbonate in sedimentary pore water[5,6], so that a change in the relative rates at which organic carbon and calcium carbonate are deposited on the sea floor should drive a compensating change in ocean pH. Here we use a model that combines ocean circulation, carbon cycling and other sedimentary processes to explore the relationship between deep-sea-sediment chemistry and atmospheric CO_2 concentration. When we include organic-carbon-driven dissolution in our model, a 40% decrease in the calcite deposition rate is enough to decrease the atmospheric CO_2 concentration to the glacial value.

‡ Present address: Department of Geophysical Sciences, 5734 South Ellis Avenue, University of Chicago, Chicago, Illinois 60637, USA.

The solubility of the calcite ($CaCO_3$) in sea water increases with pressure, so that the ocean is typically supersaturated at shallow and intermediate depths and undersaturated in the deepest waters. Only a fraction of the global calcite production is buried, and this proportion depends on the area of the sea floor that is shallower than the depth of calcite saturation. Any imbalance in the sources (terrestrial weathering and alteration) and sinks (deep sea and shallow water deposition) for $CaCO_3$ will change the ocean dissolved carbonate ion concentration ($[CO_3^{2-}]$) in the direction of restoring throughput balance. Through this mechanism, '$CaCO_3$ compensation'[2–4], the steady-state deep-sea calcite burial rate is determined by the rate of weathering less shallow water deposition, which we refer to as the 'deep-sea carbonate influx'. The pH equilibrium reaction $CO_2 + CO_3^{2-} + H_2O \leftrightarrow 2HCO_3^-$ maintains an inverse relationship between $[CO_3^{2-}]$ and pCO_2.

We simulate the coupled ocean–sediment carbon cycle using the global ocean circulation–carbon cycle model of Maier-Reimer[7,8], to which we have coupled the sediment calcite dissolution model of Archer[6]. Without the detailed sedimentary component the ocean model is unable to drive the atmospheric pCO_2 to lower glacial values without violating palaeoceanographic data[7]. Here we predict the ocean alkalinity ($[HCO_3^-] + 2[CO_3^{2-}] + [B(OH)_4^-]$) and total CO_2 ($[CO_2] + [HCO_3^-] + [CO_3^{2-}]$), rather than specifying present-day values, based on the constraint that the deep-sea calcite burial rate equals the deep-sea carbonate influx (which is imposed as a source of alkalinity and total CO_2 to the surface ocean, in the ratio of 2 : 1). The deep-sea alkalinity influx for the 'standard case' (intended to mimic present-day conditions) is 1.2 Gt-$CaCO_3$ yr^{-1} (refs 9, 10). The model distributions of alkalinity and total CO_2, and therefore the calcite saturation state of deep water, compare well with oceanic observations (Fig. 1*a* and refs 7 and 8). Although the glacial distributions of nutrients, $\delta^{13}C$

and sedimentary calcite were influenced by changes in circulation, we use the present-day ocean circulation field throughout.

The calcite diagenesis model[6] calculates the calcite dissolution rate from the steady-state concentration profiles of the carbonate species CO_2, HCO_3^- and CO_3^{2-} in the diffusive sediment pore water. Within the constraints of *in situ* microelectrode data[11], sediment trap data, pore water chemical data and calcite accumulation rates, the model predicts the observed patterns of calcite preservation in the ocean[6] (Fig. 1*b*). The steady-state sedimentary calcite distribution in the 'standard case' model is compared with observations in Fig. 2*a* and *b*. The model calcite distribution is smoother than observations because of the smoothness of the model topography.

One proposed explanation for lower glacial pCO_2 is called the 'coral reef hypothesis'[12,13]. In the present-day ocean, up to half of the total oceanic $CaCO_3$ removal may be by growth of coral reef complexes[13]. The rate of coral growth might be tied to fluctuations in sea level relative to the level of the continental shelves, with low coral growth rates during glacial times when the shelves are exposed and surface temperatures are cooler. A shift of the 'locus of $CaCO_3$ deposition' to the deep sea would require a higher ocean $[CO_3^{2-}]$, and hence a lower pCO_2 (refs 12, 13). The steady-state pCO_2 predicted by our model appears to respond linearly to variations in the deep-sea carbonate influx (Fig. 3*a* and *b*). In order for our model to achieve the magnitude of the observed glacial/interglacial pCO_2changes, the glacial deep-sea calcite burial rate has to be 2–3 times higher than today's value. Under these conditions, high-calcite sediments dominate the sea floor (Fig. 2*c*). This prediction is clearly at odds with the sedimentary record[14,15]. Although a better test of the coral-reef hypothesis would be a time-dependent calculation[13], our steady-state model is justified by the observation that the atmospheric pCO_2 recorded by the Vostok ice core was depressed to the 180 220 µatm range for 50 kyr (ref. 16). This time period is long enough for sediments to have approached their steady-state condition. Our results support the conclusion that cycles in the global growth-rate of corals would have a significant impact on pCO_2; however, we show that the coral-reef mechanism by itself cannot account for the entire glacial/interglacial pCO_2 signal.

We propose a new explanation for lower glacial pCO_2 that relies in part on the effect of sedimentary organic carbon degradation on calcite dissolution. Diagenetic models for calcite dissolution predict that a significant fraction of the calcite rain to the

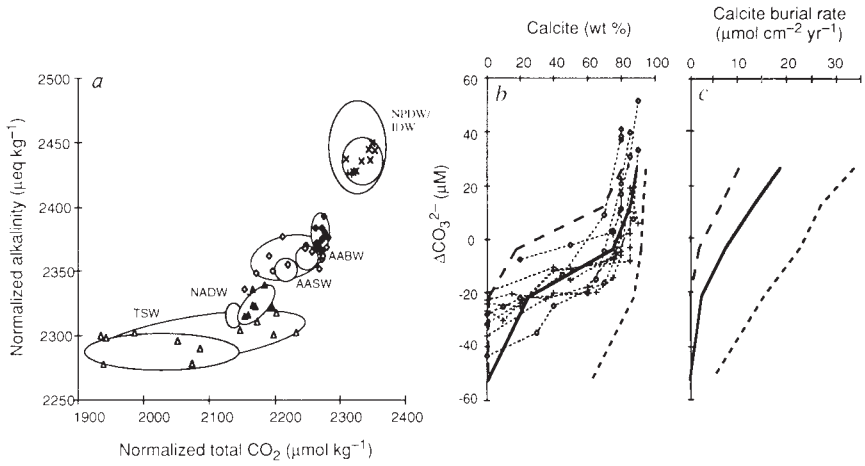

FIG. 1 *a*, Comparison of the ocean models with oceanographic data, showing the distribution of alkalinity and total CO_2 in the ocean water masses, normalized to a salinity of 35 parts per thousand. Symbols are selected data from GEOSECS[35], outlined by unshaded ovals. Shaded ovals are from the 'standard case' model runs. The model captures the general increase in dissolved carbon alkalinity with age since contact with the atmosphere, as tropical surface water is subducted into the deep sea as North Atlantic deep water, into Antarctic surface water and Antarctic deep water, to Indian and Pacific deep waters. *b* and *c*, Comparison of the sedimentary calcite preservation model[6] with oceanographic data. Vertical axis is ΔCO_3^{2-}, the saturation state of the water column with respect to calcite; because of the pressure dependence of calcite solubility[20], µM ΔCO_3^{2-} corresponds to approximately 1 km depth. Rain rates of organic carbon and calcite are from the circulation model; see above (solid line; standard case: long dashes; high organic rain: short dashes; no organic carbon rain). *b*, Calcite (dry wt%), from ref. 6. Hollow diamonds indicate summarized data from the Atlantic Ocean, crosses indicate data from the Pacific Ocean. Scatter in the data may reflect variability in organic and calcite rain rates. Calcite dissolution kinetics follow ref. 30, using a rate constant of 1 d^{-1} and a reaction order of 4.5. Organic carbon respires with O_2 according to the first-order rate constant 2×10^{-9} s^{-1}. Anoxic diagenesis is neglected. Within the sediment mixed layer (taken to be 10 cm deep), calcite is treated as well-mixed; the solid organic carbon concentration profile is calculated using a mixing coefficient of 150 cm^2 kyr^{-1}. *c*, Burial rate of calcite. By observing that the standard- and the high-organic carbon cures are similar to each other but offset by 20 µM, we can anticipate that the high-organic rain scenario will require an increase in $[CO_3^{2-}]$ of at least 20 µM to maintain constant $CaCO_3$ burial rate. Through pH equilibrium chemistry, an increase of $[CO_3^{2-}]$ of this magnitude should lead to a decrease in pCO_2 of ~20% (~60 µatm), in a homogeneous ocean. Actual global carbon cycle model response to the increase in organic rain was a $[CO_3^{2-}]$ increase of 29 µM, and a pCO_2 decrease of 55 µatm.

METHODS. For *a*, model resolution is 3.3° and the time step is one year. The rate of organic production at the surface is determined by the rate of supply of phosphate from deep water. The production of calcite is taken to be 25% of the organic carbon production on a molar basis, except in very cold waters, where calcite production is diminished[28]. The global organic carbon export production in the model is 7.3 Gt-C yr^{-1} (1 Gt is 10^{15} g). Local new production rates range from the 5 mol-C m^{-2} yr^{-1} in the equatorial Pacific to a minimum of ~0.3 mol-C m^{-2} yr^{-1} in the northeast Pacific. The rain rate of organic carbon at depth was determined based on the production rate, in the form suggested in ref. 29.

$$F_{oc} = F_{oc}(25)\,(z/100)^{-n} \quad (1)$$

where F_{oc} is the sinking flux of organic carbon at any depth, $F_{oc}(25)$ is the flux from the surface box and z is the depth in metres. The value for n is taken to be 0.7 for the standard case. The organic rain to sediments ranged from 0.02 to 0.40 mol-C m^{-2} yr^{-1}, with a global average value of 0.14 mol-C m^{-2} yr^{-1}. An analogous expression for the calcite rain rate takes the form:

$$F_{Ca} = XF_{Ca}(25) + (1-X)\,F_{Ca}(25)\,\exp(-z/2000) \quad (2)$$

where $X = 0.3$ is the proportion of the calcite production flux ($F_{Ca}(25)$) that sinks (with no attenuation) to the sediment, and the rest (0.7) dissolves in the water column with an e-folding depth of 2,000 m. The molar ratio of organic carbon flux to calcite flux (to the sediments) ranged from 0.65 to 0.8 (refs 5, 6). The sedimentary rain rate of terrigenous (refractory) material is taken to be a uniform 1.8×10^{-5} g cm^{-2} yr^{-1} over the entire pelagic see floor (with values two orders of magnitude higher in locations adjacent to the continents). The pCO_2 of the model atmosphere is determined by gas exchange with the sea surface. In order to sustain productivity in the gyres, far from areas of upwelling, the model requires sea surface nutrient concentrations that are higher than those observed (consistent with ref. 28; this tends to artificially offset the model atmospheric pCO_2 by approximately 20 µatm.

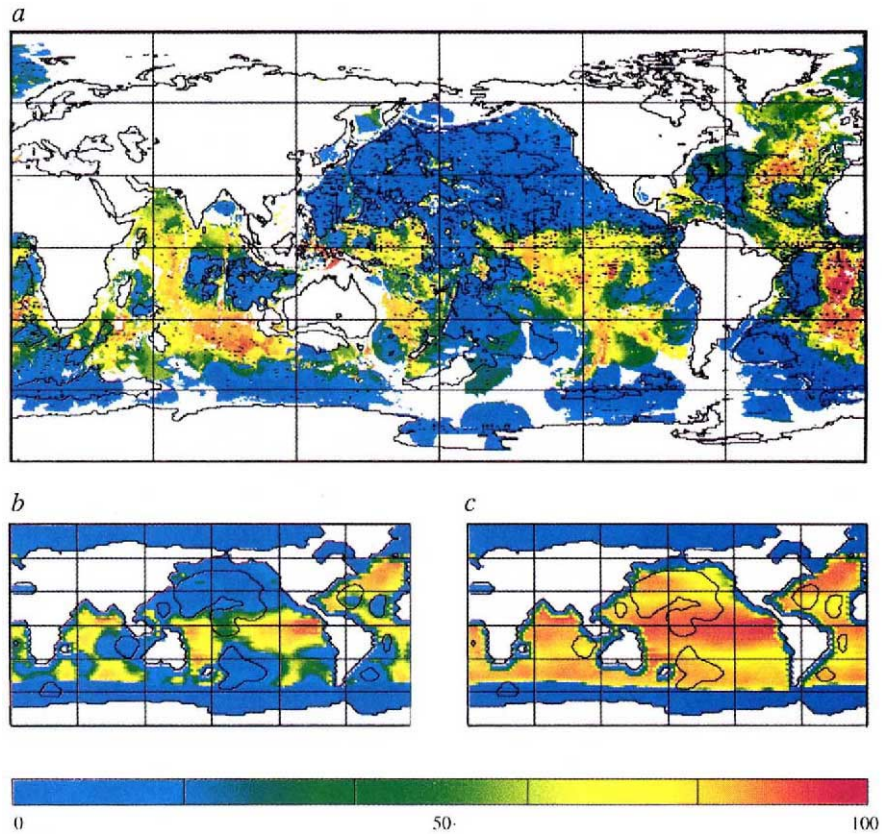

FIG. 2 Distribution of sedimentary calcite (dry wt%; see colour bar at bottom of figure); comparison of model results with oceanographic data. The contour (in *a*, *b* and *c*) indicates the 5 km isobath. *a*, An interpolation from oceanographic data[31–33]. Black dots indicate data locations. The colour field was generated using a 0.5° bathymetry and depth interpolating to the nearest data; the white fields are too far from data, in depth or horizontally, for extrapolation. *b*, Distribution of calcite predicted by the model, for the standard case. The model bathymetry is smoother than the bathymetry used to construct *a*, which results in a smoother distribution of calcite. *c*, Model distribution of calcite that results from an increased deep-sea carbonate influx (260% higher than the standard case). As sediments preserved from the last glacial maximum are not uniformly high in calcite, we conclude a lower glacial rates of shallow-water deposition is not solely responsible for low glacial atmospheric pCO_2 values.

sediments dissolves in response to the addition of CO_2 to the pore water by oxic organic carbon degradation[5,6] (a process we will refer to as 'respiratory calcite dissolution', see Fig. 1*b* and *c*). If sedimentary calcite dissolution is represented as the sum of respiratory dissolution and dissolution driven by the overlying water $[CO_3^{2-}]$, a global increase in one of these quantities will require a decrease in the other to maintain a steady state. Therefore an increase in the organic carbon/calcite ratio of the material reaching the sediments will drive an increase in $[CO_3^{2-}]$, and a corresponding decrease in pCO_2, through the mechanism of $CaCO_3$ compensation.

We test this hypothesis by altering the fraction of organic

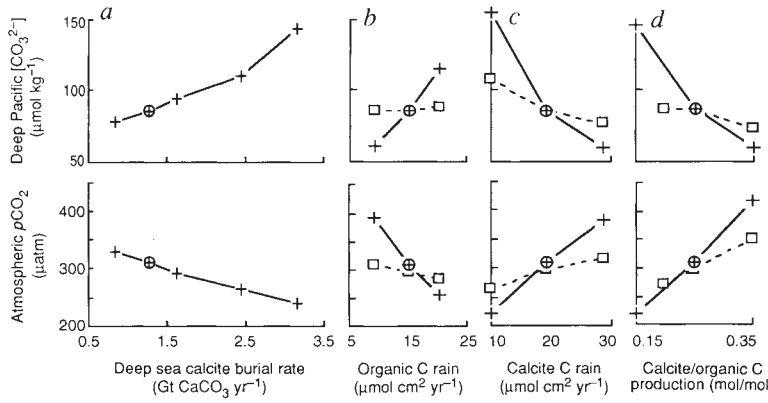

FIG. 3 Steady-state response of the coupled model to changes in the forcings for calcite burial: a comparison of results including and neglecting respiratory calcite dissolution. Upper plots are model concentration of $[CO_3^{2-}]$ in the deep Pacific (Equator and dateline, 5,000 m depth). Lower plots are atmospheric pCO_2. Solid lines with crosses are model results including the effect of organic carbon respiration in the sediments, with the 'standard case' circled; dashed lines with hollow squares are corresponding results neglecting respiratory calcite dissolution, and re-tuned to achieve a realistic lysocline and deep-sea burial rate (parameter *X* in equation (2), Fig. 1, was lowered from 0.3 to 0.07, and the dissolution rate constant was increased from 1 to 100 d^{-1}). *a*, Model response to the deep-sea carbonate influx. The distribution of calcite for the highest value used (3.1 GT–$CaCO_3$ yr^{-1}) is shown in Fig. 2c. *b*, Model response to the organic-carbon supply rate to the sea floor (average flux at 4,500 m depth). The fraction of organic carbon production that reaches the sea floor was adjusted by changing the value of *n* (equation (1), Fig. 1) from the standard value of 0.7 to 0.6 (high organic rain) and 0.85. Altering the dynamics of nutrient recycling changed the organic production rate by ±9%; however the global calcite-production rate was held to the standard value. Sensitivity of model atmospheric pCO_2 to organic-carbon sedimentary flux depends on respiratory calcite dissolution. *c*, Model response to the average calcite supply rates to the sea floor. The calcite sinking flux was adjusted by changing the value of the parameter *X* through the range (0.1, 0.3, 0.5) for the runs including organic carbon respiration, and (0.03, 0.07, 0.12) for the runs neglecting organic carbon sediment chemistry, where the middle values are the 'standard' values in each case. The effect of calcite supply is in the opposite direction to that of organic carbon: an increase of production drives an increase in pCO_2. This effect is stronger when respiratory calcite dissolution is included in the model. *d*, Model response to variation in the ratio of calcite to organic-carbon production in surface waters, with 0.25 being the standard (present-day) value. When respiratory calcite dissolution is neglected and a ratio of 0.15 is used, the sinking flux of calcite to the deep sea is insufficient to balance weathering and no steady state exists for this model. When respiratory calcite dissolution is included in the simulation, a 40% decrease in calcite production is sufficient to drive atmospheric pCO_2 close to glacial values.

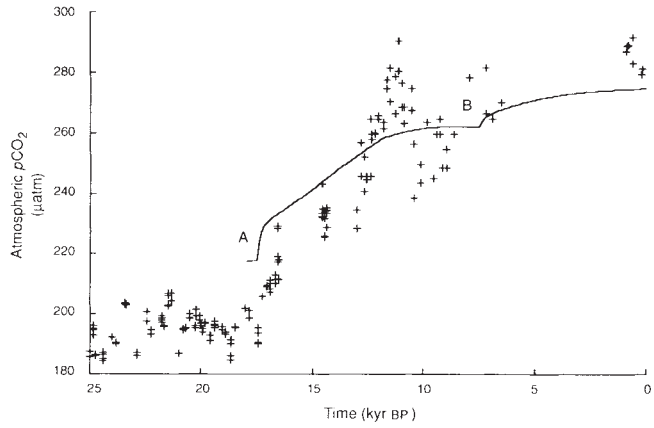

FIG. 4 Time-dependent evolution of model pCO_2 response to a 'glacial termination' scenario, compared with data from the Byrd ice core[1] plotted on the new timescale of Sowers (T. Sowers, personal communication). Initial conditions were the steady-state response to low calcite/organic carbon production rate ratio of 0.15 (Fig. 2*e*, *f*) and a reconstruction of the glacial calcite distribution (based on the generalization that calcite was preserved 350 m deeper in the glacial Pacific Ocean, 600 m shallower in the Atlantic Ocean, and the same as present day in the Indian Ocean[4]). At 17.5 kyr, the production ratio was restored to the 'standard' value of 0.25, and a 10 kyr draw-down of CO_2 by forest regrowth was initiated. The initial, fast rise in pCO_2 at 17.5–17.3 kyr BP (point A) is caused by a change in surface water chemistry; note that if surface ocean chemical rearrangement were entirely responsible for the low glacial pCO_2, the transitions would presumably be much faster than observed in the data. The sudden (artificial) end of the forst regrowth sink for Co_2 at 7.5 kyr BP (point B) can be seen in the kink in pCO_2 at that point.

carbon and calcite production that reaches the sea floor (Fig. 3*b* and *c*). As only a small fraction of production reaches the ocean bottom, altering this fraction has only a minor impact on the tracer source/sink functions in the water column. In order to isolate the effect of respiratory calcite dissolution, we ran model simulations both with and without this process. When respiratory calcite dissolution is neglected, we find that pCO_2 is sensitive to calcite rain to the sea floor, and insensitive to organic carbon rain, consistent with previously studies[17]. In contrast, when respiratory calcite dissolution is included in the simulation, pCO_2 becomes much more sensitive to organic carbon and calcite rain rates (Fig. 3*b–d*, solid lines). We also simulate an ecological shift from calcite to siliceous organisms by varying the production ratio of calcitic to organic carbon. For example, a decrease in calcite production by 40% globally drives the pCO_2 of the atmosphere near glacial values.

The required shifts in organic carbon and calcite dissolution are qualitatively supported by observations from glacial sediments. An increase in organic carbon production is suggested by an increased benthic-planktonic gradient in $\delta^{13}C$ (ref. 18), increased sedimentary organic carbon concentration[19] and burial rates[20], and a change in foraminiferal assemblages[21]. In general, calcitic organisms are replaced by siliceous diatoms in regions of high productivity and lower temperatures[22]. Both conditions are thought to be generally more prevalent under the glacial climate. In high latitudes, the front between silica and calcite production moved towards the Equator[23] during the glacial. Thus we see a general increase in organic production, and a potential shift from calcite toward siliceous production during the last glacial. We conclude that, in contrast to the coral-reef hypothesis, the requirements of a 'change in production' hypothesis seem to fit more comfortably within the constraints of the available data.

The model predicts that the alkalinity and pH of the whole ocean were higher during glacial time than at present. One test of this hypothesis will be palaeo-pH estimates derived from isotopic signature of boron[24,34] in sedimentary calcite (A. Sanyal and G. Hemming, personal communication). Another test of the hypothesis can be made by comparing model time-dependent behaviour to atmospheric pCO_2 recorded in ice cores. The ~10-kyr timescale of data from Byrd[1] is clearly longer than would be expected from a glacial/interglacial change in surface ocean chemistry[25,26] or ocean circulation[17]. The model experiment in Fig. 4 started at 18 kyr before present, (BP) with a low value for calcite production relative to organic carbon, and simulated the removal of carbon from the ocean by forest regrowth (as inferred from the $\delta^{13}C$ values of benthic foraminifera[27]) by removing 0.055 Gt-C yr^{-1} from the atmosphere, from 17.5 to 7.5 kyr BP, for a total of 550 Gt-C. The model captures the long-term behaviour of the observed CO_2 record, but misses short-term excursions (for example at 12 kyr BP) that are probably associated with fast changes in ocean circulation, sea surface temperature or terrestrial biomass, that are not simulated by the model. The model also neglects changes in terrestrial weathering intensity and coral growth that may be significant in the global alkalinity budget. We conclude, however, that the similarity between the model pCO_2 and data from Byrd supports the possibility that lower glacial pCO_2 values were caused by a higher glacial whole-ocean alkalinity. Because the 'coral reef' hypothesis (a higher deep-sea calcite burial rate during glacials) appears by itself to be inadequate as an explanation for high glacial alkalinity, we look instead to a change in the relative production rates of calcite and organic carbon. □

Received 8 February; accepted 23 November 1993.

1. Neftel, A., Oeschger, H., Staffelbach, T. & Stauffer, B. *Nature* **331,** 609–611 (1988).
2. Broecker, W. S. & Peng, T. H. *Globl Biogeochem. Cycles* **1,** 15–29 (1987).
3. Boyle, E. A. *Nature* **331,** 55–56 (1988).
4. Emerson, S. R. & Archer, D. E. *Paleoceanography* **7,** 319–332 (1992).
5. Emerson, S. & Bender, M. L. *J. mar. Res.* **39,** 139–162 (1981).
6. Archer, D. E. *J. geophys. Res.* **96,** 17037–17050 (1991).
7. Heinze, C., Maier-Reimer, E. & Winn, K. *Paleoceanography* **6,** 395–430 (1991).
8. Maier-Reimer, E. *Globl Biogeochem. Cycles* **7,** 645–678 (1993).
9. Milliman, J. D. *Marine Carbonates* 1–375 (Springer, Heidelberg, 1974).
10. Davies, T. A. & Worsley, T. R. *Paleoenvironmental Implications of Oceanic Carbonate Sedimentation Rates*, 169–179 (Spec. Publ. No. 32, Soc. Econ. Paleontologists and Mineralogists, Tulsa, 1981).
11. Archer, D., Emerson, S. & Reimers, C. *Geochim. cosmochim. Acta* **53,** 2831–2846 (1989).
12. Berger, W. H. *Naturwissenschaften* **69,** 87–88 (1982).
13. Opdyke, B. N. & Walker, J. C. G. *Geology* **20,** 733–736 (1992).
14. Berger, W. H. & Keir, R. S. in *Climate Processes and Climate Sensitivity* (eds Hansen J. E. & Takahashi, T.) 337–351 (Am. geophys. Un., Washington DC, 1984).
15. Peterson, L. C. & Prell, W. L. in *The Carbon Cycle and Atmospheric CO_2: Natural Variations Archaen to Present* (eds Sundquist E. T. & Broecker, W. S.) 251–269 (Am. Geophys. Un., Washington DC, 1985).
16. Barnola, J. M., Raynaud, D., Korotkevich, Y. S. & Lorius, C. *Nature* **329,** 408–414 (1987).
17. Keir, R. S. *Paleoooceangraphy* **5,** 253–277 (1990).
18. Sarnthein, M., Winn, K., Duplessy, J. C. & Fontugne, M. R. *Paleoceanography* **3,** 361–399 (1988).
19. Lyle, M. *et al. Paleoceanography* **3,** 39–59 (1988).
20. Lyle, M. *Nature* **335,** 529–532 (1988).
21. Mix, A. C. *Nature* **337,** 541–544 (1989). **(OK?)**
22. Lisitzin, A. P. in *The Micropaleontology of Oceans* (eds Funnell, B. M. & Reidel, W. R.) 173–195 (Cambridge Univ. Press, London, 1971).
23. Howard, W. R. & Prell, W. L. *Paleoceanography* **7,** 79–118 (1992).
24. Spivack, A. J., You, C.-F. & Smith, H. J. *Nature* **363,** 149–151 (1993).
25. Broecker, W. S. & Peng, T.-H. *Globl Biogeochem. Cycles* **3,** 215–239 (1989).
26. Sarmiento, J. L., Toggweiler, J. R. & Najjar, R. *Phil. Trans. R. Soc. Lond.* A **325,** 3–21 (1988).
27. Leuenberger, M., Seigenthaler, U. & Langway, C. C. *Nature* **357,** 488–490 (1992).
28. Bacastow, R. & Maier-Reimer, E. *Clim. Dynam.* **4,** 95–125 (1990).
29. Martin, J. H., Knauer, G. A., Karl, D. M. & Broenkow, W. M. *Deep-Sea Res.* **34,** 267–285 (1987).
30. Keir, R. S. *Geochim. cosmochim. Acta* **44,** 241–252 (1980).
31. Biscaye, P. E., Kolla, V. & Turekian, K. K. *J. geophys. Res.* **81,** 2595–2603 (1976).
32. Berger, W. H., Adelseck, C. G. & Mayer, L. A. *J. geophys. Res.* **81,** 2617–2672 (1976).
33. Kolla, V., Bé, A. W. H. & Biscaye, P. *J. geophys. Res.* **81,** 2605–2616 (1976).
34. Hemming, N. G. & Hanson, G. N. *Geochim. cosmochim. Acta* **56,** 537–544 (1992).
35. Takahashi, T., Broecker, W. S., Bainbridge, A. C. & Weiss, R. F. Tech. Rep. No. 1, CU-1-80 (Lamont–Doherty Geological Observatory, Palisades, New York, 1980).

ACKNOWLEDGEMENTS. We thank W. Broecker, S. Emerson, L. Burkle, R. Keir, M. Lyle and D. MacAyeal for discussions. This work was supported by the Lamont Doherty Earth Observatory.